Materials Today Physics 21 (2021) 100504

Contents lists available at ScienceDirect

Materials Today Physics

journal homepage: https://www.journals.elsevier.com/materials-today-physics

Recent progresses in two-dimensional Ising superconductivity

Wanying Li [a, b], Jinqiang Huang [a, b], Xiaoxi Li [c, d], Siwen Zhao [a, b, *], Jianming Lu [e, **], Zheng Vitto Han [c, d, ***], Hanwen Wang [a, b, ****]

[a] Shenyang National Laboratory for Materials Science, Institute of Metal Research, Chinese Academy of Sciences, Shenyang, 110016, PR China
[b] School of Material Science and Engineering, University of Science and Technology of China, Shenyang, 110016, PR China
[c] State Key Laboratory of Quantum Optics and Quantum Optics Devices, Institute of Opto-Electronics, Shanxi University, Taiyuan, 030006, PR China
[d] Collaborative Innovation Center of Extreme Optics, Shanxi University, Taiyuan, 030006, China
[e] State Key Laboratory for Mesoscopic Physics, School of Physics, Peking University, Beijing, 100871, China

ARTICLE INFO

Article history:
Received 14 July 2021
Received in revised form
9 August 2021
Accepted 10 August 2021
Available online 17 August 2021

Keywords:
Two dimensional
Superconductivity
Ising spin orbital coupling
Upper critical field
Topological superconductivity

ABSTRACT

Ever since its first discovery in 1911, superconductivity, which is an ordered phase of electronic state, has been regarded as one of the most fascinating topics in modern physics. Recently, remarkable advances in sample fabrication have greatly promoted the research of superconductivity, especially in the field of two-dimensional (2D) materials, where 2D Ising superconductors have sparked immense interests for their unique properties, holding promise in engineering topological superconductivity. In this review, we summarize recent works on both experimental and theoretical studies of 2D Ising superconductivity, with particular attention to the origin of Ising superconductivity as well as their novel properties. We conclude with a discussion of how these unconventional 2D Ising superconductors can play a role in the investigation of topological superconductivity, which is of potential in quantum computing.

1. Introduction

Superconductivity, as one of the macroscopic quantum phenomena, is of great significance in the field of condensed matter physics. Since the discovery of superconductivity in 1911, whether it can exist in the 2D limit has been a long debate [1]. In 1938, Alexander Shal'nikov first reported superconductivity in Pb and Sn thin films of hundreds of nanometers in a pioneering article that started the field of thin-film superconductors [2]. In 1980s, amorphous or granular superconducting films made by quenched condensation reached a sub-nanometer scale, which boosted the studies of superconductor-to-insulator quantum phase transition and Kosterlitz-Thouless-Berezinski transition. Benefited from the rapid development of molecular beam epitaxy [3–5] and Scotch-tap exfoliation [6], crystalline superconducting thin films have been the subject of intense investigations during the last two decades and many of their basic superconducting properties have been unveiled [7–16]. For example, an overview of superconductivity in 2D systems is given by Yu Saito and colleagues [17].

Two dimensional crystalline superconductors provide unprecedented opportunities to explore novel quantum phenomenon that are otherwise prohibited by either higher dimensionality or short coherence length set by disorders. Relevant topics include quantum metallic state between superconductivity and insulators [18–20], quantum Griffith singularity in the superconducting phase transition [21], superconducting field effect transistors [22,23], and so on.

* Corresponding authors. Shenyang National Laboratory for Materials Science, Institute of Metal Research, Chinese Academy of Sciences, Shenyang, 110016, PR China.
** Corresponding author.
*** Corresponding authors. State Key Laboratory of Quantum Optics and Quantum Optics Devices, Institute of Opto-Electronics, Shanxi University, Taiyuan, 030006, PR China.,
**** Corresponding author. Shenyang National Laboratory for Materials Science, Institute of Metal Research, Chinese Academy of Sciences, Shenyang, 110016, PR China.
E-mail addresses: stelody@mail.ustc.edu.cn (S. Zhao), jmlu@pku.edu.cn (J. Lu), vitto.han@gmail.com (Z.V. Han), hwwang15s@imr.ac.cn (H. Wang).

https://doi.org/10.1016/j.mtphys.2021.100504

An example is how the investigation of upper critical field in 2D crystals renews the interplay between superconductivity and spin orbital coupling (SOC). It is well known that, as for conventional superconductors, when applying a sufficiently high external magnetic field exceeding the upper critical field B_{c2}, the superconducting state transits to normal state due to the breaking of Cooper pairs via the coexisting orbital and Pauli paramagnetic mechanisms. Generally, when lowering the dimensionality of the system to the 2D limit, the orbital effect will be weakened or eliminated and B_{c2} is dominated by Pauli paramagnetic effect which is confined to the Chandrasekhar-Clogston (or Pauli) paramagnetic limit (in units of tesla), $H_p \equiv (1.86\ \mathrm{T\ K^{-1}})\ T_{c0}$ at $T = 0$ K, where T_{c0} is the superconducting transition temperature [24]. In amorphous 2D films and intercalated transition metal dichalcogenides (TMD), the significant enhancement of B_{c2} even beyond the Pauli limit **was** generally attributed to the spin randomization brought by extrinsic mechanisms, i.e. spin orbital scattering (SOS) with impurities, despite that intrinsic Rashba-type SOC **had** been well known to account for ultrahigh B_{c2} in non-centrosymmetric heavy fermion superconductors.

Recently, it is found that some 2D TMDs with the lattice structure of 2H-MX_2 (M = transition metals; X = chalcogenides) can maintain superconducting state up to magnetic field of tens of teslas, which is far beyond the Pauli limit [24–27]. While in absence of strong spin orbital scattering, an Ising pairing mechanism is proposed, which, again, is due to the non-centrosymmetric structure that leads to an Ising-type SOC. The Ising SOC pins electron spins to the out-of-plane directions, making the in-plane upper critical magnetic field far beyond the Pauli limit. In this framework, many superconductors with huge critical magnetic fields have been found in those materials with broken inversion symmetry (Fig. 1).

In this work, we briefly review recent works on the properties and applications of 2D Ising superconductors (ISC). In general, ISC can be categorized into two classes according to the origins of the Ising Zeeman field. We start by introducing the crystal structure and electronic band structure of these 2D ISC, surveying in particular spin texture around the K (K') point of the first Brillouin zone to comprehensively understand the origin of Ising superconductivity. Afterwards, we present some novel properties of 2D ISC and show how these materials can be employed in quantum engineering such as the construction of topological superconductivity.

2. Type-I 2D Ising superconductivity

2.1. Non-centrosymmetric 2H-MX_2

Recently, 2D transition metal dichalcogenides such as MoS_2 and $NbSe_2$ have triggered immense interests for their novel properties and are believed to hold tremendous applications potential in nanoelectronics and nanophotonics [28–31]. Generally, TMDs exist in the form of MX_2, these materials exist in several structural phases. Here, we mainly discuss the 2H phase of them. The unit cell of 2H-MX_2 is composed of two units where one M atom is sandwiched between two X atoms (in a X-M-X form), forming a trigonal prismatic structure stacking along the c-axis with D_{3h} symmetry [32], Fig. 2 (a). Due to the weak bonds through van der Waals interactions between interlayers, monolayer MX_2 can be isolated via mechanical exfoliation. As we know, the SOC experienced by a moving electron with momentum k is proportional to $\boldsymbol{k} \times \mathbf{E}\cdot\sigma$, where $\mathbf{E}$ is the electric field experienced by the electron and σ denoted the Pauli matrices. In 2D limit regime, the motion of electrons is restricted in the plane. Meanwhile, in monolayer 2H-MX_2, when viewed from the top, it has a honeycomb lattice structure with a broken in-plane inversion symmetry (Fig. 2 (a)) which makes the electrons experience effective in-plane electric field. Consequently, the electron spin is strongly locked to the out-of-plane orientation by an effective Zeeman field and in opposite directions for electrons with opposite momentum. Therefore, for monolayer MX_2, electrons at the K and K' valleys experience opposite effective Zeeman fields, Fig. 2 (b). This type of Zeeman field can be viewed as an Ising Zeeman field. For some superconducting 2H-MX_2, the Ising Zeeman field can protect spins of electrons in the Cooper pairs from being realigned to the in-plane direction, leading to quite large in-plane upper critical fields B_{c2} exceeding the Pauli limit by several times.

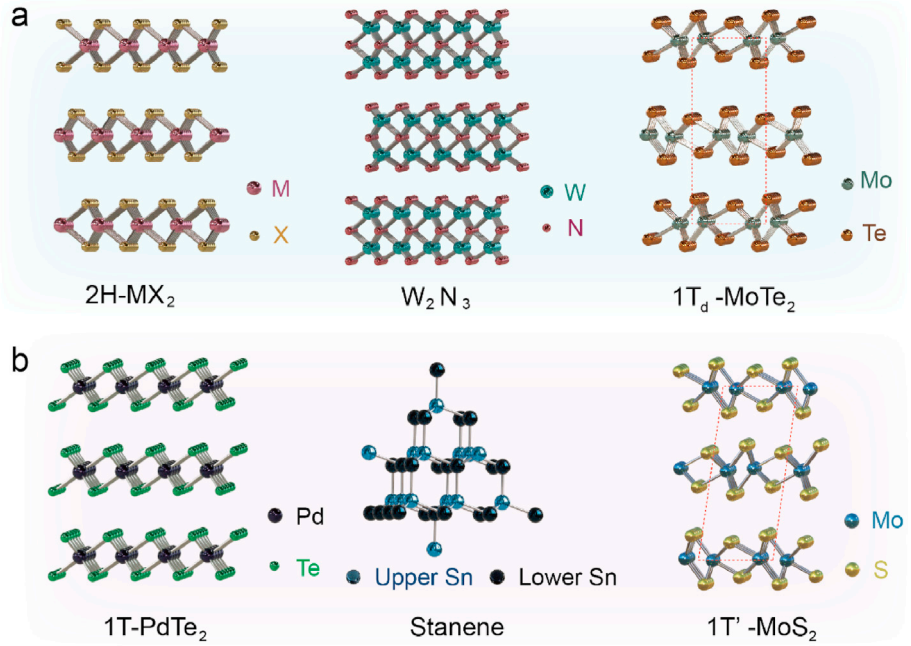

Fig. 1. The crystal structures of Type-I Ising superconductors **(a)** and Type-II Ising superconductors **(b)**.

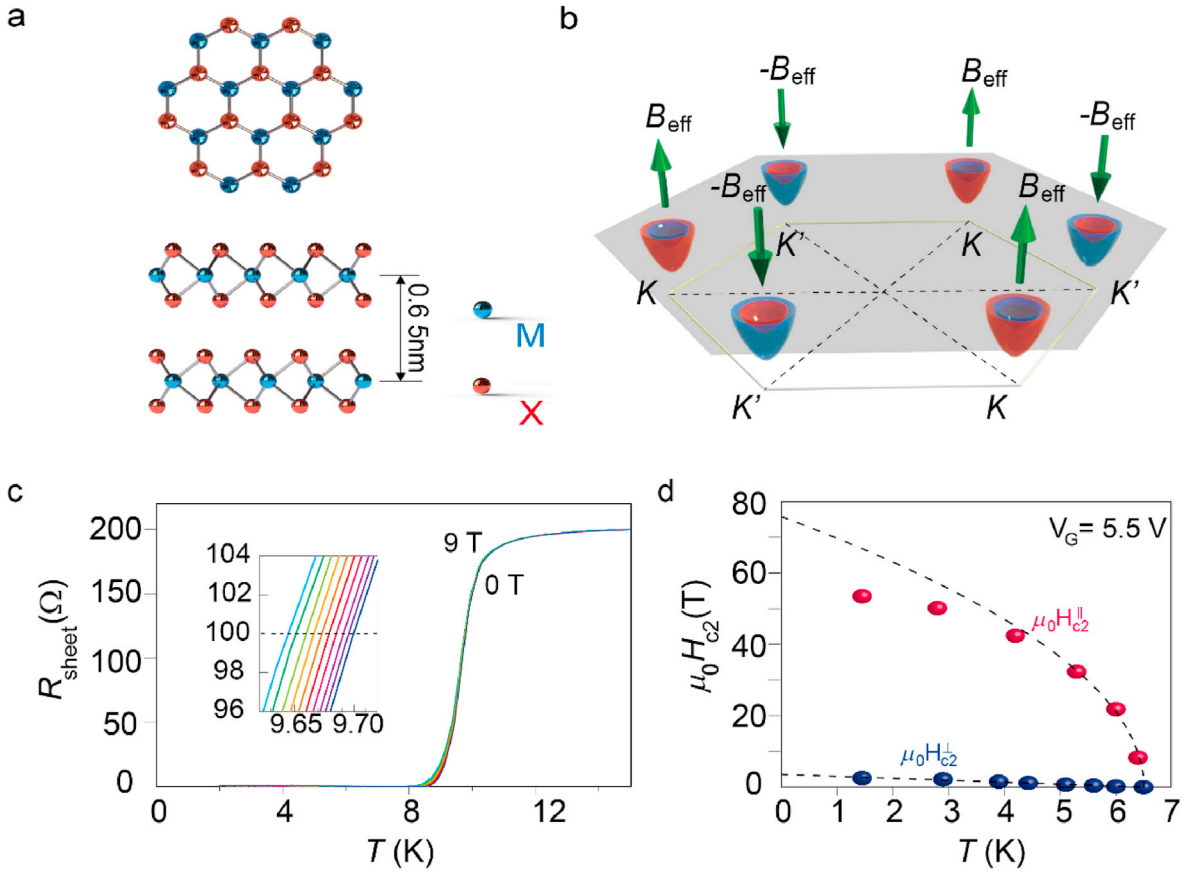

Fig. 2. **(a)** The top view (upper panel) and side view (lower view) of the crystalline structure of 2H-MX_2. **(b)** Conduction band electron pockets near the *K* and *K*′ points in the hexagonal Brillouin zone of monolayer 2H-MX_2; Adapted with permission form REF [24]. Copyright 2015, AAAS. **(c)** Temperature dependence of the resistance for an MoS_2-EDLT device under in-plane magnetic fields. **(d)** In-plane and out-of-plane upper critical fields as a function of temperature. Adapted with permission form REF [32]. Copyright 2015, Springer Nature.

Generally, non-zero electronic density of states (DOS) at the Fermi level is a precondition for superconductivity. Therefore, charge doping or gating is a widely used strategy to induce or enhance superconductivity in 2D materials [33]. In 2015, two independent groups studied the superconductivity of few-layered 2H−MoS_2 in the electric-double-layer transistor (EDLT) configuration which can create a high-density 2D electron system in the outermost layer [24,32]. It was found that the measured in-plane upper critical fields were several times higher than the Pauli limit, as shown in Fig. 2 (c, d). Spin-orbital scattering can play a role in enhancing B_{c2} in amorphous superconducting films. However, in these two works, such enhancement of B_{c2} cannot be explained by SOS as it would imply unphysically short scattering times, and they pointed out that the enhanced B_{c2} was caused by the Ising SOC, which pins the electron spins to the out-of-plane directions such that in-plane magnetic fields cannot effectively polarize electron spins to in-plane directions. These two works have attracted the attention of many scholars, and thus stimulated enormous research interests in Ising superconductivity.

Compared to the transport measurements which provide limited information about the superconducting state, the use of tunnelling spectroscopy to probe the DOS can give more information about the microscopic nature of the superconducting state. Davide Costanzo *et al.* [34] performed the tunnelling spectroscopy studies of gate-induced superconductivity in MoS_2. It is found that the vertical differential conductance exhibits a pronounced low-energy suppression, and the low-energy DOS decreases linearly with bias voltage, indicating the absence of a full gap in the superconducting state of MoS_2.

Another 2D Ising superconductor has been intensely studied is 2H−$NbSe_2$ which is believed to be a type-II s-wave superconductor with a zero-field transition temperature $T_{c0} \approx 7$ K [35–39]. 2H−$NbSe_2$ and 2H−MoS_2 have the same layered hexagonal crystal structure, in which the niobium atom is located in the center of the triangular selenium prisms. Synchronous with the discovery of Ising superconductivity in gated MoS_2, Xiaoxiang Xi *et al.* [25] studied the superconductivity in 2H−$NbSe_2$ down to monolayer limit. $NbSe_2$ is unstable in air, to provide permanent protection against degradation, they encapsulated monolayer and few-layer 2H−$NbSe_2$ by h-BN flakes in a glove box. By means of magneto-transport measurements, it was found that, superconductivity can exist in monolayer 2H−$NbSe_2$ with an ultrahigh B_{c2} exceeding 31.5 T, more than 6 times the Pauli paramagnetic limit, as can be seen in Fig. 3 (a). Besides, as the number of layer increases, the critical temperature of 2H−$NbSe_2$ increases, **but the B_{c2} decreases as interlayer coupling may destroy such Ising pairing and orbital effects become stronger.**

In conventional superconductors, a Cooper pair is a singlet state with the total S = 0. The two electron spins point in opposite directions. Whereas, the two electron spins can be aligned in the same directions, which is called spin-triplet Cooper pairs with the total S = 1. The spin-triplet superconductivity is not restricted by Pauli limit and the in-plane critical field strength could be extremely large. However, not all large violations of the Pauli limit

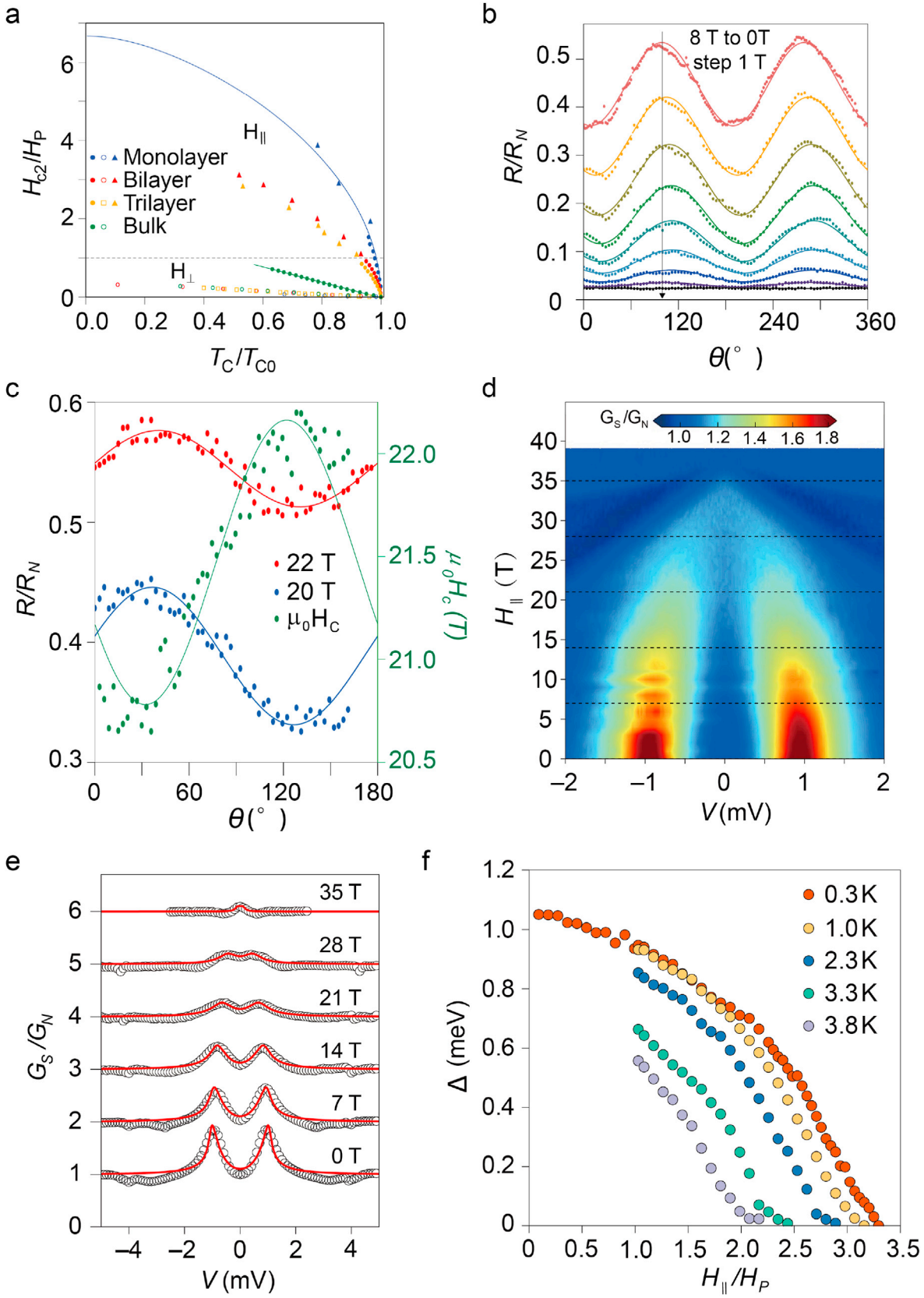

Fig. 3. **(a)** The in-plane and out-of-plane critical fields H_{C2}/H_P as a function of transition temperature T_C/T_{C0} for $NbSe_2$ samples with different thickness. Adapted with permission form REF [25]. Copyright 2015, Springer Nature. **(b)** Field dependent of the magnetoresistance for one typical $NbSe_2$ sample. **(c)** Effective critical field (green, right axis) and magnetoresistance characterization (blue and red, left axis) for a Pt/$CrBr_3$/$NbSe_2$ magnetic tunnel junction. Adapted with permission form REF [43]. Copyright 2021, Springer Nature. **(d)** Contour plot of the differential conductance of trilayer $NbSe_2$ as a function of bias voltage and in-plane field at 0.3 K. **(e)** Differential tunnelling conductance spectra at different fields (dashed lines in **(d)**). **(f)** The extracted superconducting gap as a function of $H_{\parallel}$ at various temperatures. Adapted with permission form REF [44]. Copyright 2018, Springer Nature.

are observed in spin-triplet superconductors. For example, in some atomically thin TMDs, the spin configuration of Cooper pairs consists of spin singlets. But the Ising SOC, pins the electrons spins to the out-of-plane direction and reduced the pair-breaking effect of the in-plane field. Therefore, the superconductivity in some monolayer TMDs breaks the Pauli limit. It is noteworthy that, Y Cao *et al*. has recently reported unconventional superconductivity in magic-angle twisted trilayer graphene (MATTG). They surprisingly found that the superconductivity could also survive up to a high critical field of nearly 10 T, which is about two to three times the Pauli limit. Since the spin-orbit coupling is very low and the inversion symmetry (at zero D) is not broken in graphene and twisted trilayer graphene, the origin of this unconventional superconductivity in MATTG is not the same as the atomically thin TMDs mentioned above. Some other results have also given evidence that the unconventional superconductivity in MATTG is probably spin-triplet superconductivity [40].

In addition to the mechanical exfoliation method, both chemical vapour deposition (CVD) [41] and molecular beam epitaxy (MBE) [27] can employed to prepare thin 2H−$NbSe_2$ flakes down to monolayer with high quality. Jian Wang group [27] reported that large area (over millimeters in size) of high-quality single-layer 2H−$NbSe_2$ films (0.6 nm thick) were successfully prepared on 6H−SiC(0001) substrate terminated by graphene through MBE. On this basis, to protect the 2H−$NbSe_2$ films from degradation, an amorphous Se protective layer was covered forming Se/$NbSe_2$/bilayer graphene/SiC heterostructure, and then the *ex situ* electrical transport properties of 2H−$NbSe_2$ were systematically studied. The single-layer $NbSe_2$ films show a critical transition temperature T_c^{onset} of more than 6 K and a zero-resistance temperature T_c^{zero} of up to 2.40 K, which is higher than that of the single-layer $NbSe_2$ obtained by mechanical exfoliation [25] and previous molecular beam epitaxy [42]. Moreover, low temperature and high magnetic field electrical transport measurements showed that the upper critical field B_{c2} (~32.4 T) is 5 times more than the paramagnetic limit field, which is in accordance with the ISC mechanism protected by Ising Zeeman field. In addition, measurements under vertical magnetic field at low temperature show that the monolayer 2H−$NbSe_2$ films manifest magnetic field induced superconductor-Metal transition (SMT) and the critical exponent of SMT diverge as T approaching zero, indicating quantum Griffith singularity. This is the first time that both ISC and quantum Griffith singularity have been observed in the same system. Besides, we call attention to the fact that $NbSe_2$ is an ideal platform for studying collected electronic phases because of both charge density wave (CDW) and superconductivity [42].

Very recently, the symmetry of the pairing state of few-layer $NbSe_2$ was studied under an in-plane magnetic fields [43]. Surprisingly, unlike the three-fold symmetry of the lattice, a sine-wave-like two-fold modulation of the magnetoresistance in dependence of in-plane magnetic field angle was observed in the superconducting regime as shown in Fig. 3 (b), and the field angle of minimum resistance showed dominant correction with the long, straight edge of $NbSe_2$ flakes. What's more, measurements of the effective critical filed and tunnelling across magnetic tunnel junctions also exhibit two-fold periodicity, Fig. 3 (c). Until now, the mechanism is still unclear, and a mixing scenario was proposed to understand such phenomena, that are field- or strain-induced mixing between quasi-degenerate pairing states with s-wave and d- or p-wave symmetries in few-layer $NbSe_2$ samples.

As for conventional BCS superconductors with nearly zero spin susceptibility at low temperature, the paramagnetic-limited superconductor-normal metal transition is an abrupt first-order transition at the upper critical field [42–44]. While for superconductors lacking central inversion symmetry, due to the existence of antisymmetric SOC, the spin susceptibility of the superconducting phase can become remarkable compared to the normal-state value [45,46] and lead to a continuous paramagnetic-limited transition in the zero-temperature limit. 2D ISC with atomic thickness, where the orbital effect is significantly suppressed, thus provide an ideal platform for the investigations of such paramagnetic-limited phase transition. Egon Sohn *et al.* [44] systematic investigated the superconducting gap of few-layer $NbSe_2$ by tunneling spectroscopy, and an unusual continuous paramagnetic-limited superconductor-metal transition at low temperature was observed (see Fig. 3(d–f)), providing strong evidence for significant spin susceptibility of 2D $NbSe_2$ in the zero-temperature limit.

2H-WS_2 and 2H−TaS_2 are two other recently reported 2D Ising superconductors [45,46]. 2H−TaS_2 is an intrinsic superconductor with the same crystal symmetry and similar electronic structure as $NbSe_2$, but with stronger SOC owing to the heavy Ta element [47,48]. Benjamin M. Hunt *et al.* [46] investigated the superconducting properties of 2H−TaS_2 and 2H−$NbSe_2$ in the atomic layer limit. They showed that the upper critical field was largely enhanced in monolayer 2H−TaS_2 compared to $NbSe_2$, compelling evidence of the Ising SOC origin of pairing protection in these intrinsic metallic TMDs.

Jianming Lu *et al.* [45] induced superconductivity in CVD-grown monolayer WS_2 by employing filed effect gating. Benefited from much heavier transition metal in WS_2, the Ising SOC (~30 meV) is larger than that in MoS_2 (~6 meV), leading to a more sizable enhancement of B_{c2} (about 12 times of the Pauli limit). It should be noticed that, even with larger Ising SOC, the level of Ising protection in $NbSe_2$ and TaS_2 is weaker than that in WS_2 due to the contribution of competing charge density wave phase and a spin degenerate G point [49]. What's more interesting, by increasing gate bias, they observed a transition from band insulator, superconductor, to a reentrant insulator which is attributed to localization induced by the characteristically weak screening of the monolayer.

2.2. 1T_d-$MoTe_2$

As a topological Weyl semimetal, T_d-$MoTe_2$ has attracted intensive interests recently for its intimate link between concepts of different fields of physics and material science, as well as the broad application potential [50,51]. The crystal structure of T_d-$MoTe_2$ is illustrated in Fig. 4 (a), clearly showing an alternating stacking of Te−Mo−Te triple layer structure with non-centrosymmetric space group P_{mn21} [52]. Unlike its 2H structure counterparts, both the in-plane and out-of-plane mirror symmetry of T_d-$MoTe_2$ are broken, which may provide more fascinating phenomena related to anisotropy.

By molten-salt assisted CVD method, Jian Cui *et al.* [53] synthesized high crystalline few-layer T_d-$MoTe_2$ flakes with large size and they performed low-temperature transport measurements to survey the superconducting properties of T_d-$MoTe_2$. It was found that a new type of Ising superconductivity caused by anisotropic Ising SOC exists in the material. As shown in Fig. 4 (b, c), they claimed that the in-plane upper critical field in T_d-$MoTe_2$ exceeds the Pauli limit in all planar directions but with an emergent two-fold symmetry which is different from in-plane isotropic 2D Ising superconductors. This is the first time that the in-plane anisotropic Ising superconductivity has been observed experimentally. Theo-

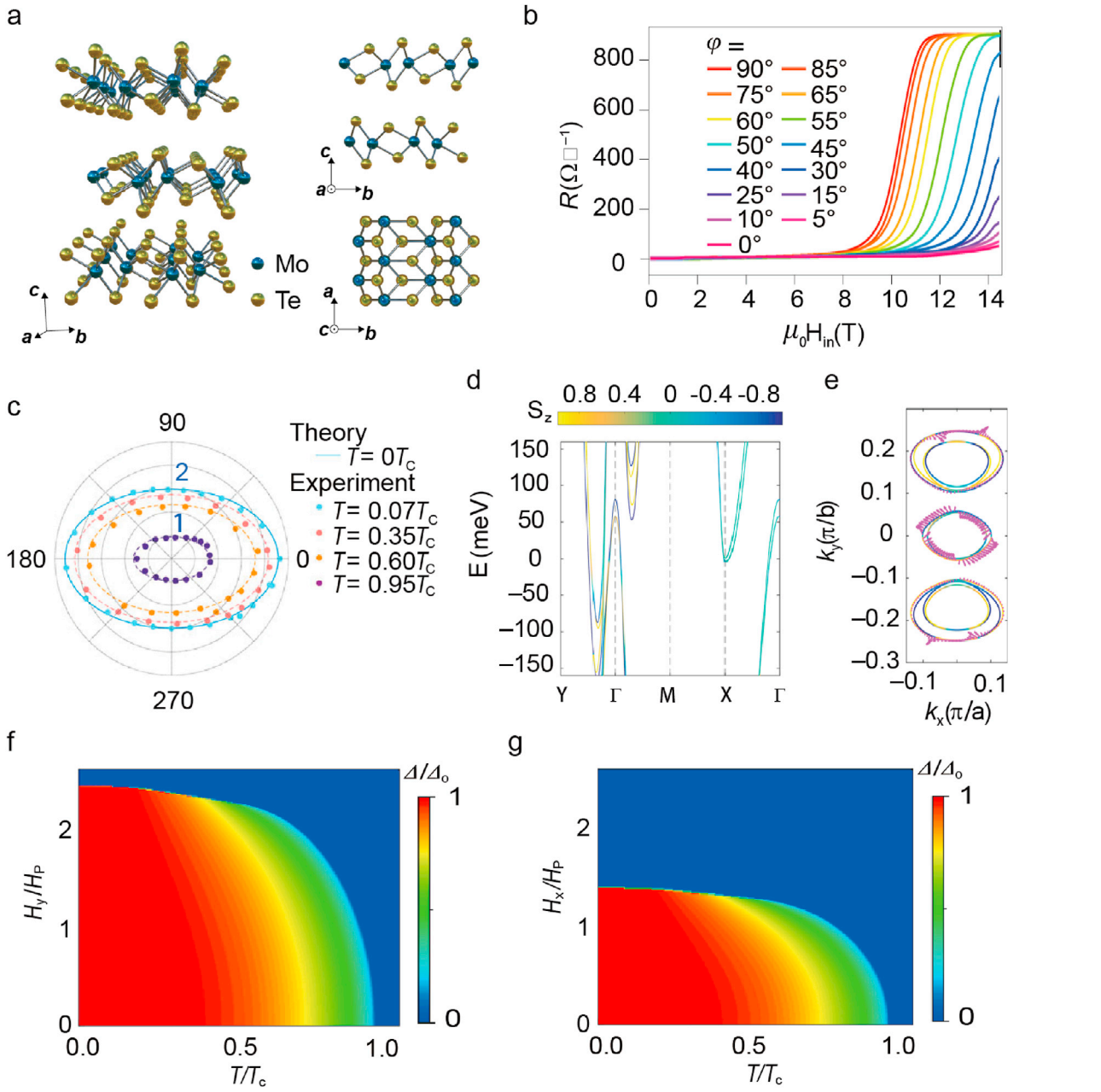

Fig. 4. Anisotropic Ising superconductivity in few layer 1T$_d$-MoTe$_2$. **(a)** Structural characterization of T_d-MoTe$_2$. **(b)** Magnetic field dependence of the sheet resistance of a 3-nm-thick MoTe$_2$ device at $T = 0.3$ K with different in-plane tilted angles. **(c)** Angular dependence of the in-plane upper critical field normalized by Pauli limit B_{c2}/B_p. The dashed lines are the asymptotic curves to show the two-fold symmetry. **(d)** The first-principle calculations for the band structure of the bilayer T_d-MoTe$_2$. **(e)** The in-plane spin texture at the Fermi level. **(f,g)** The temperature phase diagram for the superconducting state with anisotropic SOC under y- **(f)** and x- **(g)** oriented in-plane magnetic field, respectively. Adapted with permission form REF [53]. Copyright 2019, Springer Nature.

retical calculations showed that this phenomenon was due to the special lattice symmetry of T_d phase, which leads to a unique anisotropic spin orbit coupling effect. On the one hand, the breaking of the in-plane mirror symmetry in the *x* direction results in out-of-plane Ising SOC, which can effectively enhance the upper critical field B_{c2}. On the other hand, the breaking of the out-of-plane mirror symmetry gives rise to the anisotropic in-plane SOC leading to an asymmetric B_{c2}.To further confirm the asymmetric SOC enhanced B_{c2}, they calculated the band structure of bilayer T_d-MoTe$_2$ as well as the in-plane spin texture at the Fermi level. In Fig. 4 (e), the in-plane SOC is highly anisotropic at the Γ point. What's more, as can be seen in Fig. 4 (f, g), the B_{c2} along two perpendicular directions has strong anisotropy from zero temperature to near T_c as demonstrated by the mean-filed calculations. These findings give a clue that anisotropic SOC may play a role in determining the properties of 2D Ising superconductors.

2.2. 2.3 W_2N_3

W_2N_3 has been intensely studied by theoretical calculations lately, as it is believed to be an intrinsic Ising-type 2D superconductor with nontrivial topological band structure and large electron-phonon coupling (EPC) [33,54,55]. Bulk W_2N_3 has a van der Waals layered crystal structure with the space group $P6_3/mmc$

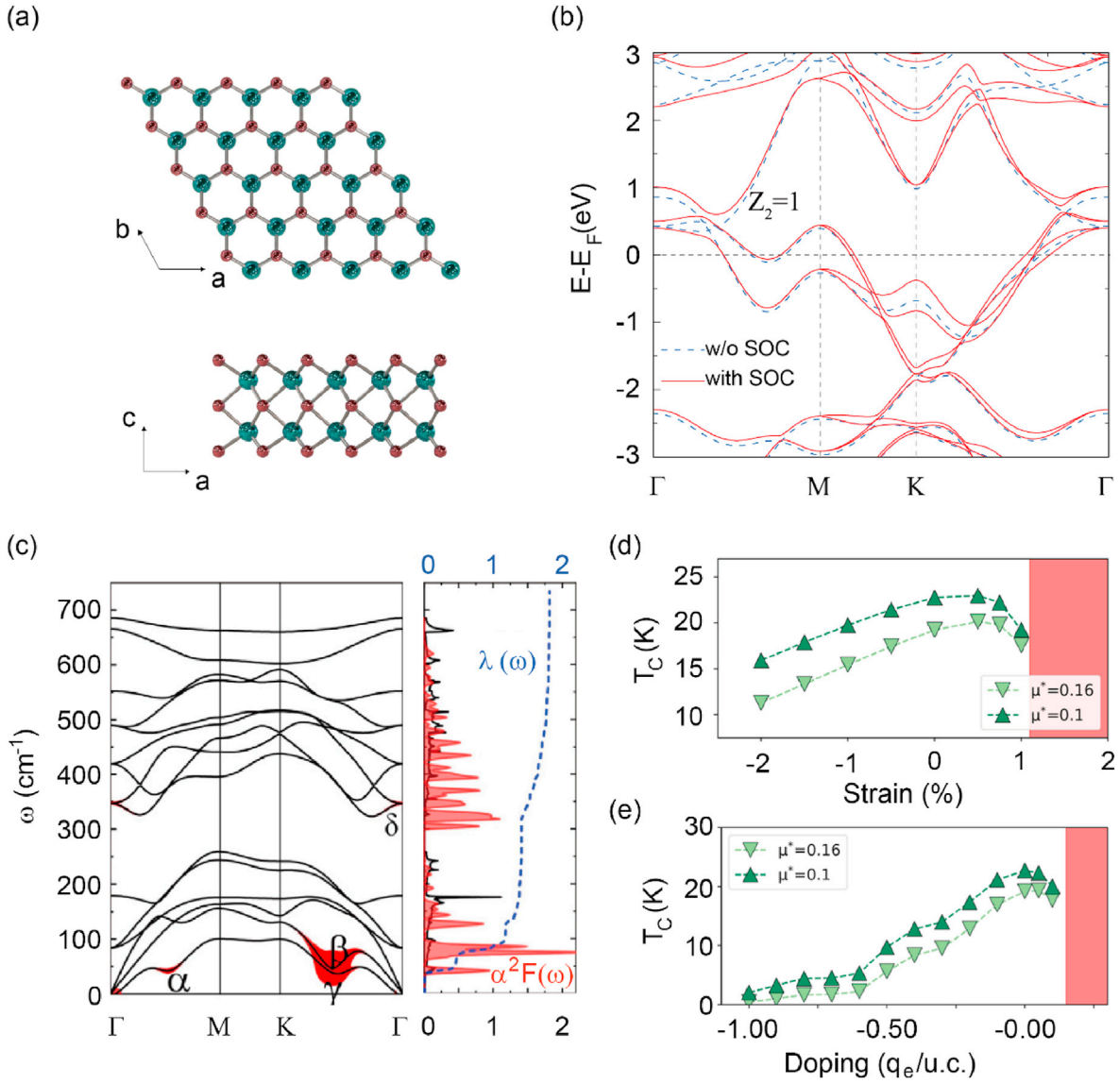

Fig. 5. **(a)** The top view (upper panel) and side view (lower view) of the crystalline structure of W_2N_3. **(b)** Electronic band structure of monolayer W_2N_3 without (dash blue lines) and with (solid red lines) SOC. Adapted with permission form REF [54]. Copyright 2021, American Physical Society. **(c)** Phonon dispersion decorated with Phonon dispersion decorated with red dots proportional to the partial EPC strength $\lambda_{q\upsilon}$. Adapted with permission form REF [33]. Copyright 2021, American Physical Society. **(d,e)** Simulated superconducting transition temperature as a function of strain **(d)** and doping **(e)** with two different μ*. Adapted with permission form REF [55]. Copyright 2021, American Chemical Society.

[56], and it possesses the inversion symmetry. Each unit cell of bulk W_2N_3 consists of two layers of W_2N_3 with W(N) atoms in one layer located precisely on top of N(W) atoms in the other layer. As for Monolayer W_2N_3, it belongs to the $P\bar{6}m2$ space group, and the W and N layers stack alternately, as illustrated in Fig. 5 (a). The out-of-plane mirror symmetry is preserved in Monolayer W_2N_3, yet the inversion symmetry is broken. Benefit from its low exfoliation energy of ~46.6 meV/atom [57], monolayer W_2N_3 can be easily exfoliated from its bulk material [58], which offers convenience for future experimental studies.

As can be seen from Fig. 5 (b), due to the relatively large SOC induced by heavy W atoms, the band structure of monolayer W_2N_3 is significantly changed and some degenerate points are varnished. Such relatively large SOC splits the degeneracy of the two states lying 0.5–0.6 eV above the Fermi level and, noticeably, it opens a nontrivial gap of 0.1 eV in the nodal line around the Γ-point, approximately 0.6 eV above the Fermi energy. It thus makes W_2N_3 a topological metal. By using density functional perturbation theory calculations through isotropical momentum-independent Eliashberg function, a large EPC constant λ of 1.815, which is mostly contributed by acoustic phonons (Fig. 5 (c)), was obtained by Jianyong Chen *et al.* Furthermore, based on the McMillian-Allen-Dynes formula, T_C is estimated to be 24.58–20.06 K with the effective screened Coulomb repulsion constant μ* from 0.10 to 0.17. Similar findings are approved by another group [54], where the EPC constant λ is calculated to be 1.47 and T_C = 21 K with μ* = 0.1. Analysis shows that such anomalous large EPC strength is originated from phonon-induced breaking of electronic degeneracies. Consequently, W_2N_3 offers an ideal platform to study the interplay between superconductivity and topological states for the coexistence of superconductivity and nontrivial band topology.

Distinct with bulk systems, 2D materials provide a greater possibility of manipulation by doping or by applying an external strain. Davide Campi *et al.* [55] studied the influence of stain and

electrical doping on the superconductivity of W_2N_3. It is found that the contraction of the lattice parameter brings a relatively slow decrease of the superconducting transition temperature, see Fig. 5 (d). As for electron doping, the T_C reduced in a moderate way, Fig. 5 (e), but it does not change the topological band structure of W_2N_3.

2.3. 2.4 Interface induced Ising superconductivity

The discovery of ISC inspires further investigations on various 2D materials. However, as most 2D superconducting systems have central inversion symmetry and cannot spontaneously generate Zeeman-protected superconductivity, the development of 2D ISC has been severely limited.

The interplay between charge, spin, orbital and lattice degrees of freedom at interfaces can give rise to a wide range of remarkable novel properties [23,59,60], which may provide a new strategy to realize the 2D ISC. Yi Liu *et al.* [61] studied the superconductivity of ultrathin Pb films grown on striped incommensurate (SIC) Pb layers on Si (111) substrates by MBE. It is found that the in-plane upper critical field of 6-ML Pb film exceeds 35.5 T at 2.8 K, which is far beyond the Pauli limit B_p (14.7 T). Since both free-standing Pb atomic layers and Si substrate have central inversion symmetry, the Zeeman-protected superconductivity in this system should originate from the interface between them. Different from the hexagonal close-packed structure in a free-standing Pb atomic layer, the Pb layer in the SIC phase is distorted which can extend to the neighboring Pb layers as demonstrated by first-principle calculations. Such lattice distortion breaks the in-plane inversion symmetry and gives rise to Zeeman-type SOI in ultrathin Pb film on SIC. Such results may provide a new perspective to expand the material matrix available for 2D ISC.

3. Type-II ising superconductivity

For a long time since its first discovery, Ising superconductivity has been considered to exist only in materials with broken space inversion symmetry. However, unconventional superconducting behavior has been uncovered recently in 1T′-MoS_2 which retains the inversion symmetry, with the in-plane upper critical field far exceeds the Pauli paramagnetic limit (Fig. 6 (b, c)) [62]. The spin-valley locking and Rashba spin-orbit interaction are rule out to interpret the H_{c2} enhancement because of the centrosymmetric structure in 1T′-MoS_2 nanosheets (Fig. 6 (a)). In particular, the H_{c2}/H_p in 1T′-MoS_2 is smaller than $MoTe_2$ with similar thickness,

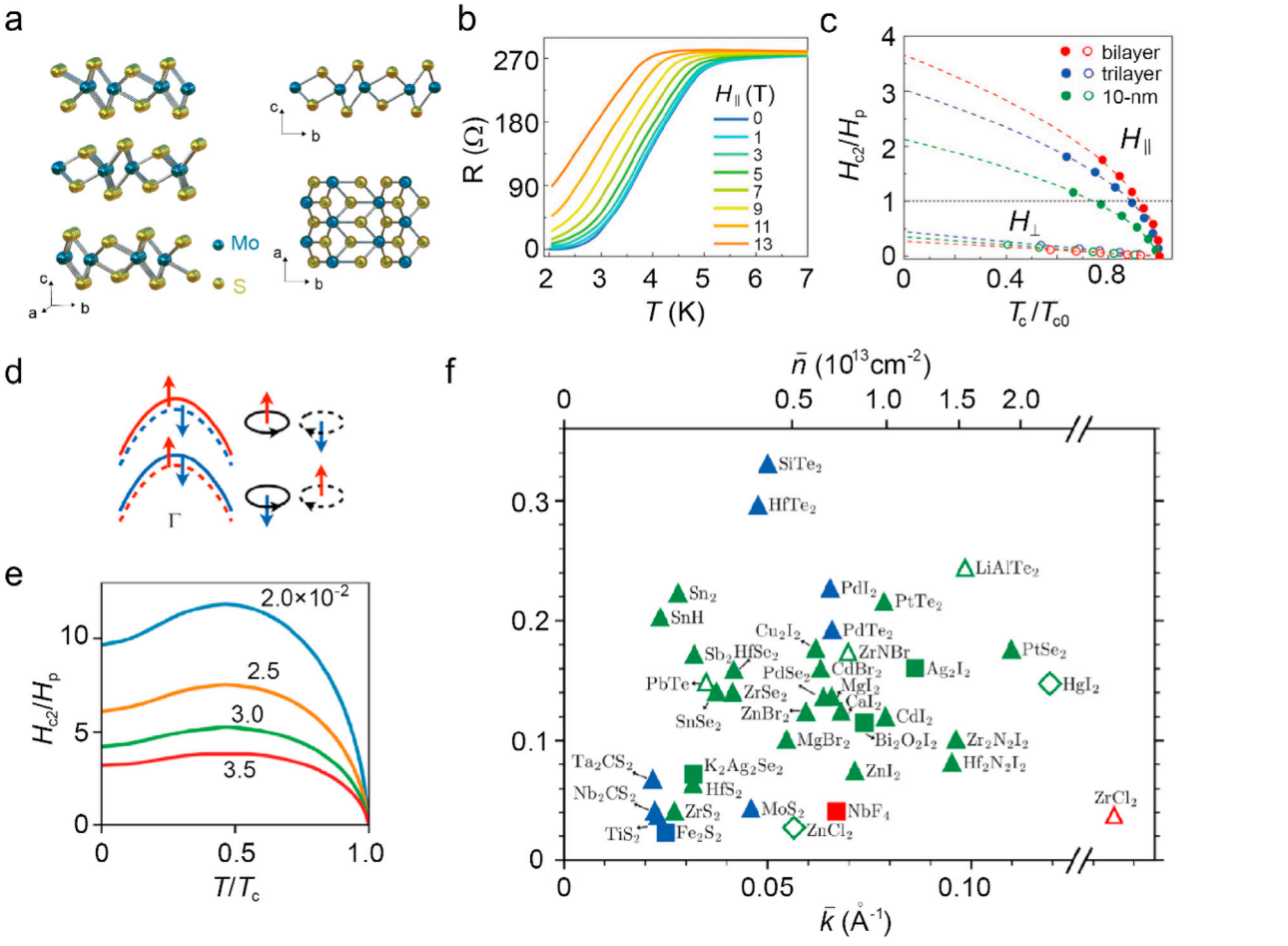

Fig. 6. **(a)** Atomic model of 1T′-MoS_2. **(b)** Temperature dependence of resistance for trilayer sample under parallel magnetic fields. **(c)** The H_{c2}/H_p as a function of T_c/T_{co} for 1T′-MoS_2 samples with different thickness. The solid dots represent H_{c2} under parallel field and the hollow dots under perpendicular field. The dash line is the fit for 2D Ginzburg-Landau model. Adapted with permission form REF [62]. Copyright 2019, Wiley-VCH. **(d)** Schematic picture of type-II Ising superconductivity. Near Γ, spin-up and spin-down are locked to the two opposing orbitals (denoted by solid and dashed lines, respectively). They spit in energy for each orbital by a Zeeman-like field, whose sign is opposite for opposing orbitals. The dashed and solid lines are degenerate in energy. **(e)** The relation between critical field B_{c2}, normalized by Pauli limit B_p, with respect to temperature T, normalized by critical temperature T_c. **(f)** Candidate materials of type-II Ising superconductors. Blue markers indicate the relevant bands cross the intrinsic Fermi energy, and green (red) markers indicate the relevant bands are below (above) the intrinsic Fermi energy. Solid (hollow) markers indicate inversion symmetric (asymmetric) materials. Triangular, rectangular, and rhombic markers correspond to C_3, C_4, S_4 symmetric materials. Adapted with permission form REF [63]. Copyright 2019, American Physical Society.

suggesting spin-orbit interaction plays significant role. Therefore, further research is required to understand the mechanism of anomalous enhancement of H_{c2} in 2D 1T′-MoS_2.

In 2019, Yong Xu *et al.* [63] proposed a new type of Ising superconductivity mechanism, *i.e.* the second type of Ising superconductivity without destroying the space inversion symmetry, based on 2D materials with multiple degenerate orbitals. In 2D materials with lattice inversion symmetry, energy degeneracy (such as in-plane P_{XY} orbit) will appear in the orbit of electrons, which provides the possibility to explore new physics of spin orbit coupling. Due to the spin orbit coupling effect, the clockwise and counterclockwise in-plane electron orbit will produce effective magnetic fields perpendicular to the plane in opposite directions. Owing to such intrinsic magnetic field, the electron spin is polarized, and the direction of polarization is out of the plane. In centrosymmetric materials, despite the spin degeneracy, the electrons with opposite spin are bound to the orbit with reverse motion, leading to a so-called spin-orbital locking, and the direction of the intrinsic magnetic field felt by the electrons with different orbits is opposite (Fig. 6 (d)). Meanwhile, in materials with heavy elements, SOC can produce ultrahigh intrinsic magnetic fields up to thousands of teslas, which can effectively resist the external in-plane magnetic field perpendicular to it. Therefore, superconductivity can survive in strong in-plane magnetic field in this kind of material system, i.e. type-II Ising superconductors. The theoretical calculation results showed that the upper critical field H_{c2} of these type-II Ising superconductors is much higher than that of general superconductors, which can significantly break through the Pauli limit (Fig. 6 (e)). Besides, based on high-throughput first-principles calculations, a large number of Ising superconductor candidates are predicted, as can be seen in Fig. 6 (f), which can be used for subsequent experimental verifications and practical applications.

3.1. Stanene

The superconductivity of tin has been studied for more than 100 years, but only exists in white tin (β - Sn). Another common phase of tin is gray tin (α - Sn), which is a semi metal and has no superconductivity. In recent years, α - Sn has been recognized as a topological insulator. Yong Xu and Shousheng Zhang [64,65] predicted that the single layer α − Sn (111), namely stanene, which has a hexagonal structure similar to graphene may hold significant topological properties such as quantum spin Hall effect at room temperature. Fig. 7 (a) illustrates the lattice structure of stanene, the atomic arrangement of stanene follows the hexagonal honeycomb structure of graphene but with a buckled form, which is due to the sp^2-sp^3 hybridization of Sn atoms [66,67].

In 2018, Qikun Xue *et al.* [68] successfully obtained flat thin α - Sn films with high quality by means of MBE on lead tellurium (PbTe) terminated silicon (111) substrate. Following electric and magnetic transport measurements at low temperature revealed that 2D superconductivity existed in thin α - Sn films down to 2 atomic layers, which is the first time to find superconductivity in gray tin. The results show that the density of state of stanene is

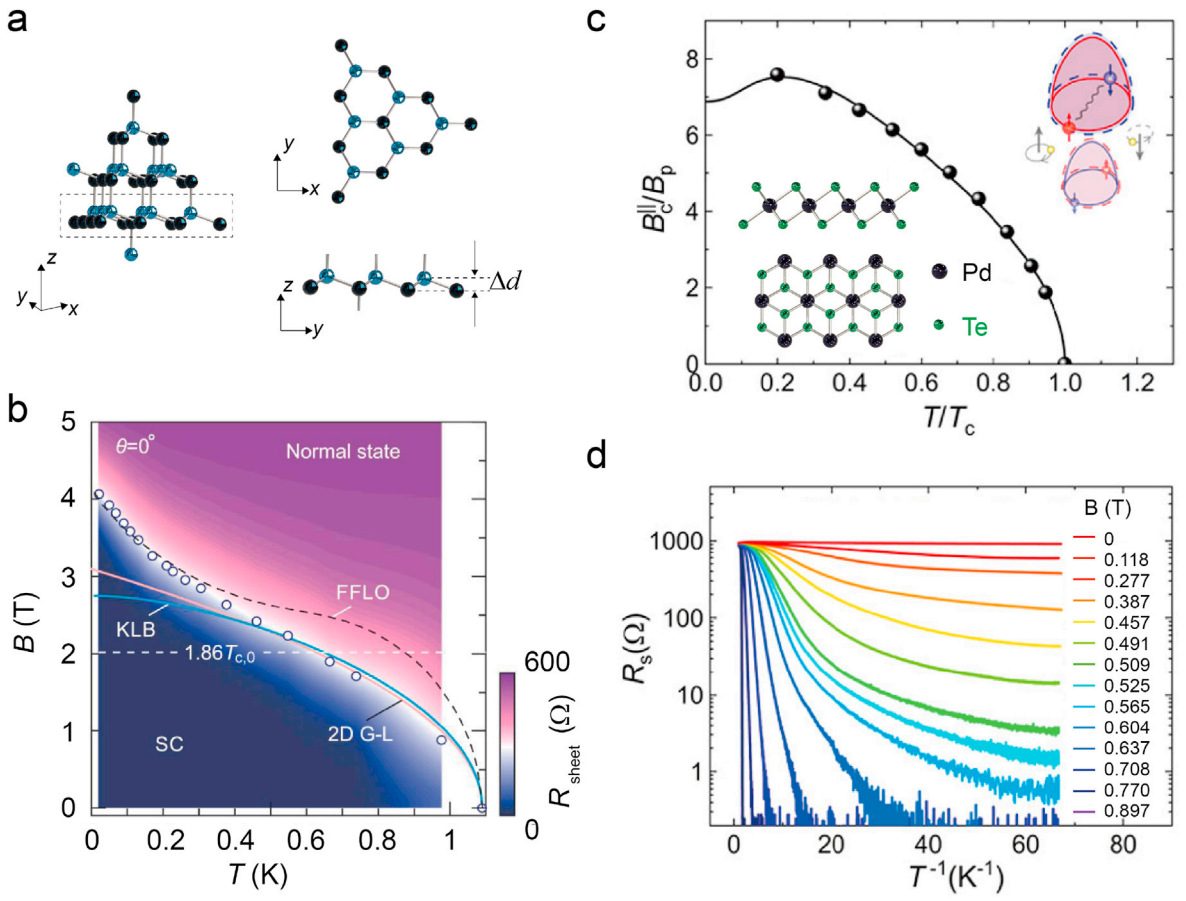

Fig. 7. **(a)** Lattice structure of stanene, the Sn atoms in upper/lower level are represented by blue and black balls respectively. **(b)** Temperature dependence of the in-plane upper critical fields in few-layer stanene samples. Adapted with permission form REF [70]. Copyright 2020, AAAS. **(c)** Theoretical fitting of B_c/B_p *vs* T/T_c using a fixed Zeeman-type SOC and increasing effective Rashba-type SOC. The inset shows the atomic model of $PdTe_2$. **(d)** Arrhenius plot of the sheet resistance at different perpendicular magnetic fields from 0 to 0.897 T. Adapted with permission form REF [74]. Copyright 2020, American Chemical Society.

modulated by the substrate, which leads to the appearance of superconductivity. By changing the substrate thickness, they also realized the transition from single band superconductor to double band superconductor.

Very recently, Joseph Falson *et al.* [70] systematically investigated the superconductivity in few layer Stanene (α-Sn) with high lattice symmetry and demonstrated the experimental observation of type-II Ising superconductivity. They carried out in-situ rotation measurements under high magnetic field at low temperature and the behavior of the critical magnetic field of the samples with different thicknesses in the whole superconducting temperature range was systematically measured. It was found that the in-plane upper critical field exceeds the Pauli limit by a factor of 2, Fig. 7 (b). What's more, the divergent behavior of the critical magnetic field when the temperature approaches to absolute zero has been clearly observed, which is a typical evidence of Ising superconductivity.

3.2. 1T-$PdTe_2$

$PdTe_2$ is known to become a superconductor below $T_c = 1.7$ K and has attracted a lot attention for having both superconductivity and type-II Dirac fermions, which makes it an ideal platform for exploring novel physics [71,72]. It is a layered material of a CdI_2-type structure ($P\bar{3}m1$) with in-plane inversion symmetry [73], as shown in the inset of Fig. 7 (c). Recently, systematic transport studies on the ultrathin $PdTe_2$ films grown on $SrTiO_3$ (001) substrate by MBE were performed by Jian Wang group [74]. It is found that the H_{c2} of these ultrathin crystalline $PdTe_2$ films are more than 7 times the Pauli limit as confirmed by magnetoresistance measurements, see Fig. 7(c). Besides, the temperature dependence of $B_c^{\parallel}$ normalized by B_p fits well with the theoretical formula for Ising superconductor, indicating the enhancement of B_{c2} may originate from Zeeman-protected Ising superconductivity. First-principles calculations reveals that the protecting of Zeeman-type SOC mainly comes from the band close to the Γ point. Due to the spin-orbital locking, which is introduced by SOC, the effective Zeeman field $\beta_{SO}\tau_z$ (β_{SO} represents the Zeeman-type SOC strength and $\tau_z = \pm 1$ label $p_x \pm ip_y$ orbitals) shows opposite signs for the $p_x \pm ip_y$ orbitals. What's more, as ensured by the C3 rotational symmetry, the direction of effective Zeeman field is out-of-plane, and its magnitude can be extraordinarily large due to the strong SOC. As a consequence, the electron spins are thus strongly polarized along the out-of-plane direction. What's more interesting, there is an anomalous metallic state exists in $PdTe_2$ as characterized by the resistance saturation at low temperatures in a perpendicular magnetic field, shown in Fig. 7(d).

4. Interactions with magnetism

Generally, superconductivity and magnetism are two antipathetic condensed matters because of the opposing requirement on electron spin configuration. However, fascinating phenomena may appear when they are bound together, including unconventional superconductivity and topological superconductivity [75–77]. The atomically sharp interfaces between 2D layered Ising superconductor and magnetic materials presents an ideal platform to explore new phenomena from coexisting superconductivity and magnetic ordering.

$CrBr_3$ is a ferromagnetic semiconductor with out-of-plane anisotropy [78]. Kaifeng Kang *et al.* [79] carried out tunneling spectroscopy studies of $NbSe_2/CrB_3/NbSe_2$ tunnel junctions. Thanks to the extremely high upper critical fields of $NbSe_2$, the magnetization of $CrBr_3$ can be tuned to in plane by a relatively small in-plane magnetic field without decoupling the Cooper pairs in $NbSe_2$. As investigated via field-dependent tunneling spectroscopy, when the in-plane magnetic field is increased to 1 T, which is much higher than the in-plane saturation field, giant magnetoresistance (~100%) appears near the coherence peak (Fig. 8 (a, b)), which is originated from Spin-dependent interactions. What's more striking, as shown in Fig. 8 (c), a hysteresis behavior is observed albeit there is no hysteresis in the $CrBr_3$ magnetization. Such phenomenon is not understood up to now, further in-depth studies are needed.

As a phase difference ϕ develops between two superconductors, a DC Josephson supercurrent $I_s = I_c \sin(\phi)$ flows through the junction, where the critical current I_C is the maximum supercurrent that can exist through the Josephson junction (JJ). As can be obtained from the above formula, the vanishing supercurrent at the minimum energy imposes the condition that only $\phi = 0$ or π. For conventional superconductors with spin-singlet pairing, the spatially symmetric Cooper pair wavefunction enforces $\phi = 0$ as the ground state. However, when two superconductors are connected across a ferromagnet (F), the transferred Cooper pairs can acquire an additional phase when tunneling through the magnetic barrier due to magnetic exchange interaction, yielding a spatial oscillation of the superconducting order parameter in the barrier [80–82]. As a result, for certain thickness of the F-barrier, the sign of the superconducting order parameter across the barrier can be reversed caused by an exchange-energy driven phase shift [80,83–85], resulting in a π-phase JJ. What's more, a parallel arrangement of 0- and π−JJ can lead to a degenerate φ-JJ, which holds promise in the application of superconducting quantum electronic devices [86–91].

Recently, the coupling between Ising superconductivity and magnetism has attracted much attentions. P. Kim *et al.* [92] demonstrated the engineering of doubly degenerate φ-JJs in a vdW system using an atomically thin $NbSe_2$ Ising superconductor and the domain structure in the ferromagnetic semiconductor $Cr_2Ge_2Te_6$ to form a coherent combination of 0 and π JJ segments. $Cr_2Ge_2Te_6$ is a vdW ferromagnetic semiconductor with out-of-plane spin orientation, whose Curie temperature was found to be about 64 K [93]. To probe the Josephson phase, they combined one $NbSe_2/Cr_2Ge_2Te_6/NbSe_2$ F-JJ with one reference JJ ($NbSe_2/NbSe_2$) to realize SQUID, and the edges of the top and bottom $NbSe_2$ flakes were aligned to each to each other, which allows momentum-conserving tunneling in such vdW heterostructures. The measured maximal SQUID critical current $I_{SQUID}^{C}(\Phi)$ shows oscillations with the periodicity $\Phi_0 = h/2e$. While in the field range of ±1.2 mT, an irregular SQUID response was observed (Fig. 8 (d)), with a telegraph-like signal oscillating between two metastable critical current branches, which may indicate of a doubly degenerate ground state of such system. Besides, measurements of the switching current reflect that none of the switching schemes provide 0 or π phase but $\varphi_{c-} = 259°$ and $\varphi_{c0} = 59°$ as shown in Fig. 8 (e). These findings imply that two switching current states exist in such structure, which is also observed by Linfeng Ai *et al.* [94].

Due to the special spin configuration of $NbSe_2$ induced by inversion symmetry breaking, the Josephson phase between Ising Cooper pairs (ICPs) on the surfaces of $NbSe_2$ across the ferromagnetic barrier can be sensitively modified by the magnetization direction. As illustrated by 8 (f), for out-of-plane magnetization, the spin of the ICPs is aligned parallel or anti-parallel with the spin of the MI, resulting in a negative sign of the wave function of ICPs tunneling across the F-JJ, which sets the phase of the JJ ground state to be $\phi = \pi$ [95]. On the contrary, for the magnetization deviate from the out-of-plane direction, the spin of the ICPs can flip during

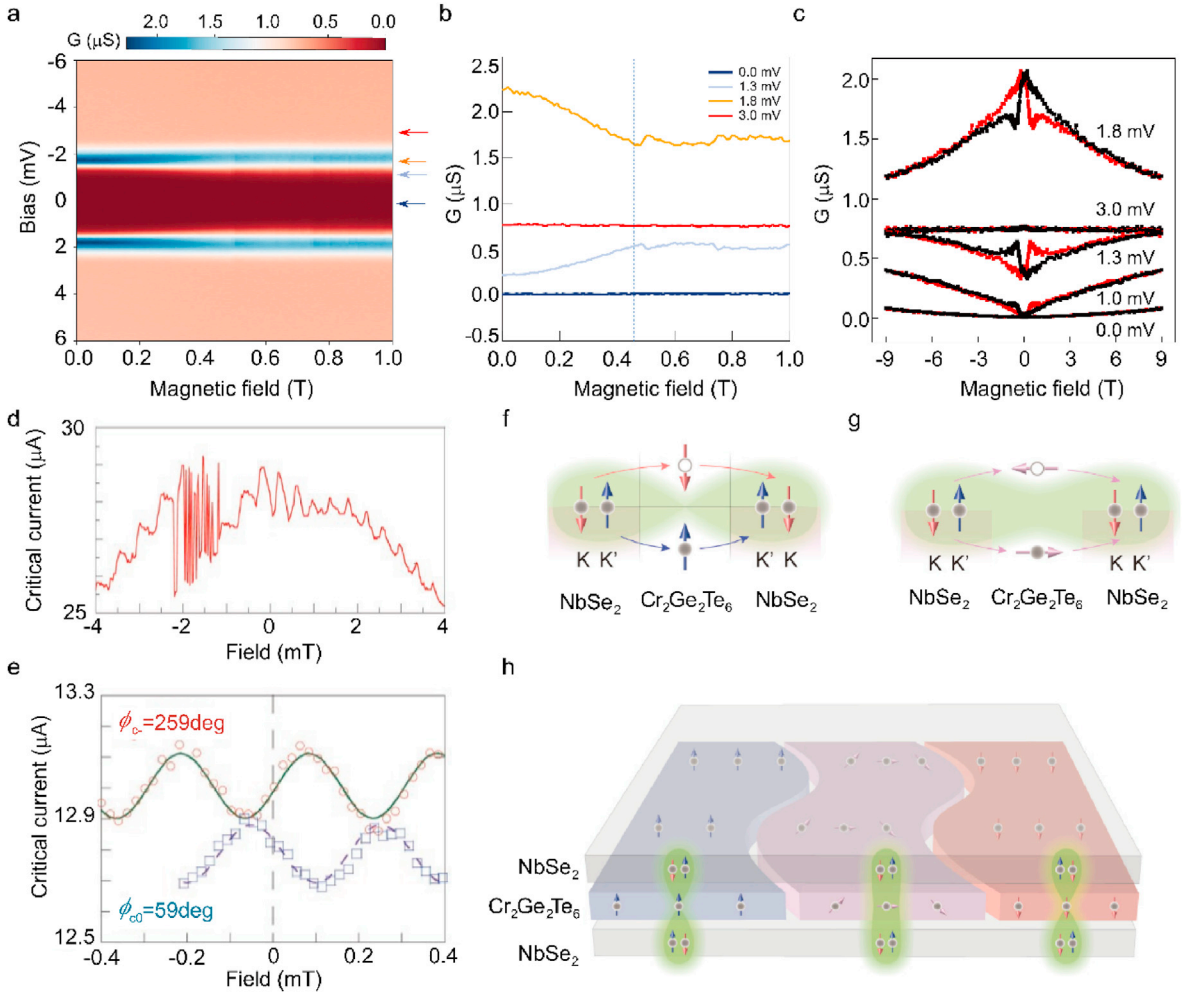

Fig. 8. **(a)** Contour plot of tunneling spectrum as a function of in-plane field. **(b)** Differential conductance as a function of magnetic field at selected DC bias voltages. **(c)** Magnetic hysteresis of differential conductance at selected DC bias voltages at 1.5 K. **(d)** The SQUID oscillates with telegram-like critical current between the fields of −1.1 mT and −2.2 mT, which implies the presence of two metastable state. **(e)** The $Cr_2Ge_2Te_6$-SQUID oscillation. **(f–h)** Illustration of the Ising-Cooper-pair coupling through the magnetic tunneling junction for perpendicular magnetization **(f)**, for in-plane magnetization **(g)**, and for magnetic multi-domain structure **(h)**.

the tunneling process, leading to the ground state of the Josephson junction to be $\phi = 0$. As a result, due to the multi-domain state in few layer $Cr_2Ge_2Te_6$, a degenerate φ-JJ is realized in $NbSe_2$/$Cr_2Ge_2Te_6$/$NbSe_2$ vdW heterostructures, as shown in Fig. 8 (g).

5. Attempts to create topological superconductivity

Topological superconductors and Majorana fermions (MFs) are highly desirable from fundamental and technological views and have triggered enormous interest in recent years [96–98]. MFs are like to exist as quasiparticle excitations which are their own anti-particles in certain condensed matter systems [99]. As MFs are non-Abelian anyons, particle exchanges are non-trivial operations. That is to say, different from other known particle types where an exchange operation merely has the effect of multiplying the wave-function with $+1$ (for bosons) or -1 (for fermions), or a general phase factor φ (for 'ordinary' (Abelian) anyons) [100–102]. Exchange the position of MFs thus does not depend on the method or details of the execution, which is topologically protected and only depends on the exchange statistics of quasiparticles, leading to the potential applications in the fault-tolerant topological quantum computation [103].

Systems simultaneously exhibiting superconductivity and spin–orbit coupling are predicted to provide a route toward topological superconductivity and unconventional electron pairing, driving significant contemporary interests in these materials [46]. Here, we will survey some recent works on engineering topological superconductivity and realizing MFs in 2D Ising superconducting systems.

Due to its distinctive spin orbital coupling effect, soon after the discovery of 2D Ising superconductivity, researchers proposed that it might be used to engineering topological superconductivity [104–108].

In 2016, Benjamin T. Zhou *et al.* [104] theoretically reported that Ising SOC in 2D Ising superconductors might introduce equal-spin-triplet Cooper pairs with spin polarized to the in-plane directions. It is showed that, by solving the Gor'kov equations, they obtained the pairing correlations matrix of the 2D Ising superconductor defined as:

$$F_{\alpha\beta}(\boldsymbol{k}, E) = -i\int_0^{\infty} e^{i(E+i0^+)t}\{C_{\boldsymbol{k},\alpha}(t), C_{-\boldsymbol{k},\beta}(0)\}dt$$

where α, β are the spin indices. For a new spin quantization axis which forms an angle θ with the z-axis, the paring correlations

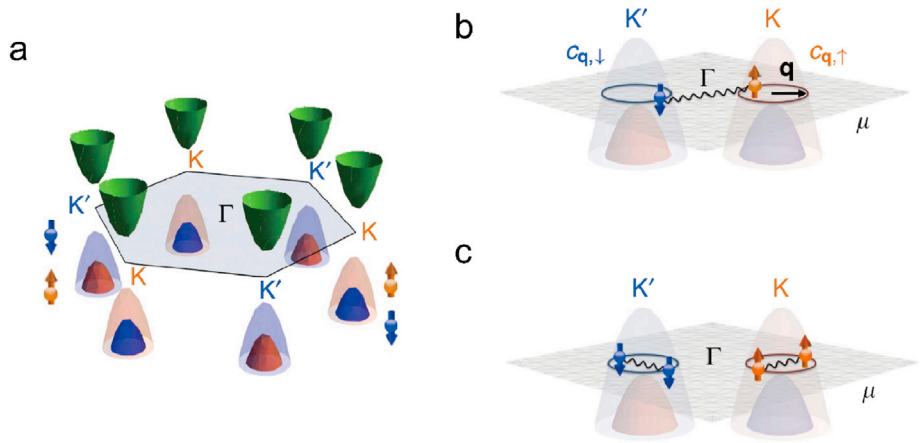

Fig. 9. **(a)** The schematic low-energy dispersion of a monolayer TMD. The green paraboloids represent the nearly spin-degenerate conduction band, and the orange and blue paraboloids represent the spin-split valence bands for the spin-up and -down electrons, respectively. **(b, c)** Two different type of pairing: interpocket pairing **(b)** and intrapocket pairing **(c)**. $c_{q,\uparrow}$ ($c_{q,\downarrow}$) denotes the annihilation operator for spin-up (-down) electrons on the pocket at valley *K* (*K*′), and q denotes the momentum relative to the pocket centres. Adapted with permission form REF [107]. Copyright 2017, Springer Nature.

become:

$$F_\theta(\boldsymbol{k}, E) = \begin{pmatrix} -d_z \sin\theta & \Psi_s + d_z \cos\theta \\ -\Psi_s + d_z \cos\theta & d_z \sin\theta \end{pmatrix}$$

where Ψ_s labels the spin-singlet pairing correlation amplitude, and d_z is the spin-triplet pairing correlation amplitude, which is generated by Ising SOC. For spin quantization axis fixed along the *x* direction with $\theta = \pi/2$, all the triplet Cooper pairs are formed by equal-spin electron pairs with spins pointing to the in-plane directions. Therefore, Cooper pairs can tunnel into the in-plane polarized half metal (electrodes) without suffering severe suppression. More importantly, they pointed out that, when placed a half-metal wire on top of a 2D Ising superconductor, the spin-triplet Cooper pairs could induce superconducting pairings in the wire, resulting in a one-dimensional (1D) topological superconductor with Majorana end states.

Stimulated by this work, research groups began to search for topological superconductivity in 2D Ising superconducting systems. It was found later that, beside the half-metal wires, a chain of magnetic impurities may also create topological superconducting states and thus Majorana fermion excitations in 2D Ising superconductors. Usually, in a superconducting system, magnetic impurities do harm to pairing and as a result sub-gap bound states known as Yu-Shiba-Rusinov (YSR) states emerge [109–111]. By introducing a single magnetic impurity, Girish Sharma and Sumanta Tewari [105] discussed properties of YSR states on superconducting MoS_2 surface. It was found that the magnetic field response of STM zero bias peaks (ZBP) induced by YSR states is strongly anisotropic in the presence of Ising SOC. Further, they predicted the emergence of a topological superconducting phase with zero energy MFs excitations for a chain of magnetic impurities with moments parallel (or have a parallel component) to the plane of 2D Ising superconductors. Almost at the same time, another independent group also demonstrated similar predictions, that is, Ising superconductors can support a topological superconducting state in the YSR chain, as long as the magnetic moments have a finite in-plane component [106]. Both works indicate that 2D Ising superconductor is an ideal system for searching topological superconductivity and MFs.

In addition to the above proximity-induced pairing, monolayer TMDs itself can also lead to pairing possibilities for topological superconductivity. Yi-Ting Hsu *et al.* [107] theoretically studied lightly hole-doped monolayer TMDs, and they proposed a new strategy to realize topological superconductivity: to split the spin degeneracy of fermions in momentum space. Due to the broken inversion symmetry, the system goes through Ising SOC which acts as opposite Zeeman fields on the two valleys. Besides, the Ising SOC is orbital-selective and selectively affects the valence band with a large spin-split. Fig. 9 (a) depicts the low-energy dispersion of a monolayer TMD with the orange and blue paraboloids represent the spin-split valence bands for the spin-up and -down electrons, respectively. As a result, spin-valley-locked fermions can be achieved near the two valleys when the TMDs are slightly p-doped (Fig. 9 (b, c)). It is shown that such spin-valley locking in hole-doped TMDs together with repulsive interactions selectively favours two topological superconducting states: interpocket paired state with Chern number 2 and intrapocket paired state with finite pair momentum.

Recently, Wen-Yu He *et al.* [108] reported that, by applying an in-plane magnetic field which is higher than the Pauli limit but lower than B_{c2}, monolayer 2H−$NbSe_2$ and other superconducting TMDs can be driven to nodal topological superconductors. Deferent from Mo- and W- based materials, the chemical potential of $NbSe_2$ lies in the valence band and the band splitting is still robust at the Fermi energy even though the Fermi surface is far away from the *K* points, which is critical to create the nodal topological phase. In the nodal topological phase, bulk nodal points located on Γ−M lines where the Ising SOC vanishes are created by an in-plane magnetic field and these nodal points are connected by Majorana flat bands.

6. Conclusion and perspectives

As a summarization, 2D Ising superconductivity has been a growingly new topic in condensed matter physics. In this short review, we have briefly gone through recent progresses in the investigations of 2D Ising superconductivity in various material systems, including metallic elemental superconductors, TMDs, and Weyl semimetals. The spin-valley and/or spin-orbital locking mechanism has led to emerging physical phenomena such as largely enhanced in-plane critical field, which may find applications for superconductivity under high magnetic fields. In the meantime, 2D Ising superconductors are predicted to be an ideal platform for the investigations of quantum devices such as topological superconductors that take advantage of the parafermions such as MFs. Currently, the possible schemes for realizing MFs are

proposed in semiconductor nanowire/superconductor and quantum anomalous Hall/superconductor heterostructures. Recently, Wen-Yu He *et al.* [112] predicted that the in-plane magnetic field can easily drive the phase transition toward a nodal topological superconductivity in monolayer TMD, which is possibly an accessible way to realize MFs. However, despite these intense theoretical works, experimental realization of topological superconductivity is still in its infancy. Novel materials as well as their nanostructures are yet to be discovered experimentally for the advancement in the research of Ising superconductivity. Besides, as mentioned in part IV, heterostructures between Ising superconductors and ferromagnetic films have been proven to be the platforms performing fruitful physics [113]. Therefore, more theory predictions and experiments based on heterostructures are needed for the unraveling of new physical phenomena. Last but not least, as theories have proposed that type II Ising superconductivity can be realized in diverse candidate materials, yet it is of great challenges to push one step further toward the demonstration of applications based on the quantum braiding of proximity induced topological superconductor from spin-triplet Cooper pairs.

Declaration of competing interest

All authors declare no competing interests.

Acknowledgments

This work is supported by the National Key R&D Program of China (2019YFA0307800) and the National Natural Science Foundation of China (NSFC) (Grants 11974357 and U1932151). S. Z. acknowledges support from the NSFC (grant 12004259). X. L. acknowledges support from the NSFC (grant 12004389).

References

[1] K. Ghosh, H. Rahaman, P. Bhattacharyya, IEEE Trans. Appl. Supercond. 30 (2019) 1–9.
[2] A. Shalnikov, Nature 142 (1938) 74, 74.
[3] Y. Guo, Y.F. Zhang, X.Y. Bao, T.Z. Han, Z. Tang, L.X. Zhang, W.G. Zhu, E.G. Wang, Q. Niu, Z.Q. Qiu, Science 306 (2004) 1915–1917.
[4] N. Reyren, S. Thiel, A.D. Caviglia, L.F. Kourkoutis, G. Hammerl, C. Richter, C.W. Schneider, T. Kopp, A.-S. Rüetschi, D. Jaccard, M. Gabay, D.A. Muller, J.-M. Triscone, J. Mannhart, Science 317 (2007) 1196–1199.
[5] A. Gozar, G. Logvenov, L.F. Kourkoutis, A.T. Bollinger, L.A. Giannuzzi, D.A. Muller, I. Bozovic, Nature 455 (2008) 782–785.
[6] K.S. Novoselov, A.K. Geim, S.V. Morozov, D. Jiang, Y. Zhang, S.V. Dubonos, I.V. Grigorieva, A.A. Firsov, Science 306 (2004) 666–669.
[7] D. Eom, S. Qin, M.Y. Chou, C.K. Shih, 027005, Phys. Rev. Lett. 96 (2006) 1, 027005.4.
[8] A. Gozar, G. Logvenov, L.F. Kourkoutis, A.T. Bollinger, I. Bozovic, ChemInform (2009) 40.
[9] S. Qin, J. Kim, Q. Niu, C.-K. Shih, Science 324 (2009) 1314–1317.
[10] N. Reyren, S. Thiel, A.D. Caviglia, L.F. Kourkoutis, G. Hammerl, C. Richter, C.W. Schneider, T. Kopp, A.-S. Rueetschi, D. Jaccard, Science 317 (2007) 1196–1199.
[11] N.E. Staley, J. Wu, P. Eklund, Y. Liu, L. Li, Z. Xu, Phys. Rev. B 80 (2009) 184505.
[12] Z. Tong, C. Peng, W.J. Li, Y.J. Sun, G. Wang, X.G. Zhu, H. Ke, L. Wang, X. Ma, C. Xi, Bull. Chin. Acad. Sci. 25 (2011) 301–303.
[13] K. Ueno, S. Nakamura, H. Shimotani, A. Oht0Mo, N. Kimura, T. N0Jima, H. A0Ki, Y. Iwasa, M. Kawasaki, Nat. Mater. 7 (2008) 855–858.
[14] Q.Y. Wang, Z. Li, W.H. Zhang, Z.C. Zhang, J.S. Zhang, W. Li, H. Ding, Y.B. Ou, P. Deng, K. Chang, Chin. Phys. Lett. 108 (2012): 037402.
[15] G. Yang, Y.F. Zhang, X.Y. Bao, T.Z. Han, T. Zhe, L.X. Zhang, W.G. Zhu, E.G. Wang, N. Qian, Z.Q. Qiu, Science 306 (2004) 1915–1917.
[16] J.T. Ye, S. Inoue, K. Kobayashi, Y. Kasahara, H.T. Yuan, H. Shimotani, Y. Iwasa, Nat. Mater. 9 (2010) 125–128.
[17] Y. Saito, T. Nojima, Y. Iwasa, Nature Reviews Materials 2 (2016) 16094.
[18] Yu, Yuichi Saito, Jianting Kasahara, Yoshihiro Ye, Tsutomu Iwasa, Nojima, *Science* 350 (2015) 409–413.
[19] A.W. Tsen, B. Hunt, Y.D. Kim, Z.J. Yuan, S. Jia, R.J. Cava, J. Hone, P. Kim, C.R. Dean, A.N. Pasupathy, Nat. Phys. 12 (2015) 208–212.
[20] C. Yang, Y. Liu, Y. Wang, L. Feng, Q. He, J. Sun, Y. Tang, C. Wu, J. Xiong, W. Zhang, X. Lin, H. Yao, H. Liu, G. Fernandes, J. Xu, J.M. Valles, J. Wang, Y. Li, Science 366 (2019) 1505–1509.
[21] Y. Xing, H.-M. Zhang, H.-L. Fu, H. Liu, Y. Sun, J.-P. Peng, F. Wang, X. Lin, X.-C. Ma, Q.-K. Xue, J. Wang, X.C. Xie, Science 350 (2015) 542–545.
[22] C.H. Ahn, S. Gariglio, P. Paruch, T. Tybell, L. Antognazza, J.-M. Triscone, Science 284 (1999) 1152–1155.
[23] A.D. Caviglia, S. Gariglio, N. Reyren, D. Jaccard, T. Schneider, M. Gabay, S. Thiel, G. Hammerl, J. Mannhart, J.M. Triscone, Nature 456 (2009) 624–627.
[24] J.M. Lu, O. Zheliuk, I. Leermakers, N.F.Q. Yuan, U. Zeitler, K.T. Law, J.T. Ye, Science 350 (2015) 1353–1357.
[25] X. Xi, Z. Wang, W. Zhao, J.H. Park, K.T. Law, H. Berger, L. Forró, S. Jie, K.F. Mak, Nat. Phys. 12 (2016) 139–143.
[26] A.W. sn, Y.D. Hun, Km, Z.J. Yuan, S. Ja, R.J. Cava, J. Hon, P. Km, C.R. Dan, A.N. Pasupahy, Nat. Phys. 12 (2016) 208.
[27] Y. Xing, K. Zhao, P. Shan, F. Zheng, Y. Zhang, H.L. Fu, Y. Liu, M. Tian, C. Xi, H. Liu, Nano Lett. 17 (2017) 6802–6807.
[28] K.F. Mak, K. He, C. Lee, G.H. Lee, J. Hone, T.F. Heinz, J. Shan, Nat. Mater. 12 (2013) 207–211.
[29] Q.H. Wang, K. Kalantar-Zadeh, A. Kis, J.N. Coleman, M.S. Strano, Nat. Nanotechnol. 7 (2012) 699–712.
[30] Y. Zhang, J. Ye, Y. Matsuhashi, Y. Iwasa, Nano Lett. 12 (2012) 1136–1140.
[31] B. Radisavljevic, A. Radenovic, J. Brivio, V. Giacometti, A. Kis, Nat. Nanotechnol. 6 (2011) 147–150.
[32] Y. Saito, Y. Nakamura, M.S. Bahramy, Y. Kohama, J. Ye, Y. Kasahara, Y. Nakagawa, M. Onga, M. Tokunaga, T. Nojima, Nat. Phys. 12 (2016) 144–149.
[33] J. Chen, Y. Ge, Phys. Rev. B 103 (2021): 064510.
[34] D. Costanzo, H. Zhang, B.A. Reddy, H. Berger, A.F. Morpurgo, Nat. Nanotechnol. 13 (2018) 483–488.
[35] S. Foner, E.J. Mcniff, J.R. Gavaler, M.A. Janocko, Phys. Lett. 45 (1974) 429.
[36] P.D. Trey, S. Gygax, J.P. Jan, J. Low Temp. Phys. 11 (1973) 421–434.
[37] H.F. Hess, R.B. Robinson, R.C. Dynes, J.M.V. Jr, J.V. Waszczak, Phys. Rev. Lett. 62 (1989) 214.
[38] C.L. Huang, J.Y. Lin, Y.T. Chang, C.P. Sun, H.Y. Shen, C.C. Chou, H. Berger, T.K. Lee, H.D. Yang, Phys. Rev. B 76 (2007) 4692, 4692.
[39] T. Yokoya, T. Kiss, A. Chainani, S. Shin, M. Nohara, H. Takagi, Science 294 (2001) 2518–2520.
[40] Y. Cao, J.M. Park, K. Watanabe, T. Taniguchi, P. Jarillo-Herrero, Nature 595 (2021) 526–531.
[41] H. Wang, X. Huang, J. Lin, J. Cui, Y. Chen, C. Zhu, F. Liu, Q. Zeng, J. Zhou, P. Yu, Nat. Commun. 8 (2017) 394.
[42] M.M. Ugeda, A.J. Bradley, Y. Zhang, S. Onishi, Y. Chen, W. Ruan, C. Ojeda-Aristizabal, H. Ryu, M.T. Edmonds, H.-Z. Tsai, Nat. Phys. 12 (2016) 92–97.
[43] A. Hamill, B. Heischmidt, E. Sohn, D. Shaffer, K.-T. Tsai, X. Zhang, X. Xi, A. Suslov, H. Berger, L. Forró, Nat. Phys. 2021, 1-6.
[44] E. Sohn, X. Xi, W.-Y. He, S. Jiang, Z. Wang, K. Kang, J.-H. Park, H. Berger, L. Forró, K.T. Law, Nat. Mater. 17 (2018) 504–508.
[45] J.M. Lu, O. Zheliuk, Q.H. Chen, I. Leermakers, N.E. Hussey, U. Zeitler, J.T. Ye, Proc. Natl. Acad. Sci. Unit. States Am. 115 (2018) 3551.
[46] S.C.D.L. Barrera, M.R. Sinko, D.P. Gopalan, N. Sivadas, B.M. Hunt, Nat. Commun. 9 (2018) 1427.
[47] E. Navarro-Moratalla, J.O. Island, S. Ma, as-Valero, E. Pinilla-Cienfuegos, A. Castellanos-Gomez, J. Quereda, G. Rubio-Bollinger, L. Chirolli, J.A. Silva-Guillén, N. Agraït, et al., Nat. Commun. 7 (2016) 11043.
[48] J. Pan, C. Guo, C. Song, X. Lai, H. Li, W. Zhao, H. Zhang, G. Mu, K. Bu, T. Lin, X. Xie, M. Chen, F. Huang, J. Am. Chem. Soc. 139 (2017) 4623.
[49] R.A. Klemm, Physica C Superconductivity & Its Applications 514 (2015) 86–94.
[50] A. Tamai, Q.S. Wu, I. Cucchi, F.Y. Bruno, S. Riccò, T.K. Kim, M. Hoesch, C. Barreteau, E. Giannini, C. Besnard, Phys. Rev. X 6 (2016): 031021.
[51] T.R. Chang, S.Y. Xu, G. Chang, C.C. Lee, M.Z. Hasan, Nat. Commun. 7 (2016) 10639.
[52] J. Jiang, Z.K. Liu, Y. Sun, H.F. Yang, C.R. Rajamathi, Y.P. Qi, L.X. Yang, C. Chen, H. Peng, C.-C. Hwang, Nat. Commun. 8 (2017) 13973.
[53] J. Cui, P. Li, J. Zhou, W.-Y. He, X. Huang, J. Yi, J. Fan, Z. Ji, X. Jing, F. Qu, Nat. Commun. 10 (2019) 2044.
[54] J.-Y. You, B. Gu, G. Su, Y.P. Feng, Phys. Rev. B 103 (2021) 104503.
[55] D. Campi, S. Kumari, N. Marzari, Nano Lett. 21 (2021) 3435–3442.
[56] S. Wang, X. Yu, Z. Lin, R. Zhang, D. He, J. Qin, J. Zhu, J. Han, L. Wang, H.-k. Mao, Chem. Mater. 24 (2012) 3023–3028.
[57] N. Mounet, M. Gibertini, P. Schwaller, D. Campi, A. Merkys, A. Marrazzo, T. Sohier, I.E. Castelli, A. Cepellotti, G. Pizzi, Nat. Nanotechnol. 13 (2018) 246–252.
[58] H. Yu, X. Yang, X. Xiao, M. Chen, Q. Zhang, L. Huang, J. Wu, T. Li, S. Chen, L. Song, Adv. Mater. 30 (2018) 1805655.
[59] A. Tsukazaki, A. Ohtomo, T. Kita, Y. Ohno, H. Ohno, M. Kawasaki, Science 315 (2007) 1388.
[60] N. Reyren, S. Thiel, A.D. Caviglia, L.F. Kourkoutis, G. Hammerl, C. Richter, C.W. Schneider, T. Kopp, A.S. Rueetschi, D. Jaccard, Science 317 (2007) 1196–1199.
[61] Y. Liu, Z. Wang, X. Zhang, C. Liu, Y. Liu, Z. Zhou, J. Wang, Q. Wang, Y. Liu, C. Xi, Phys. Rev. X 8 (2018): 021002.
[62] J. Peng, Y. Liu, X. Luo, J. Wu, Y. Xie, Adv. Mater. 31 (2019) 1900568.
[63] C. Wang, B. Lian, X. Guo, J. Mao, Z. Zhang, D. Zhang, B.-L. Gu, Y. Xu, W. Duan, Phys. Rev. Lett. 123 (2019) 126402.
[64] J. Wang, Y. Xu, S.-C. Zhang, Phys. Rev. B 90 (2014): 054503.
[65] Y. Xu, B. Yan, H.J. Zhang, J. Wang, G. Xu, P. Tang, W. Duan, S.C. Zhang, Phys.

Rev. Lett. 111 (2013) 136804, 1-136804.5.
[66] X. Chen, R. Meng, J. Jiang, Q. Liang, Q. Yang, C. Tan, X. Sun, S. Zhang, T. Ren, Phys. Chem. Chem. Phys. 18 (2016) 16302–16309.
[67] S. Balendhran, S. Walia, H. Nili, S. Sriram, M. Bhaskaran, Small 11 (2015) 640–652.
[68] M. Liao, Y. Zang, Z. Guan, H. Li, Y. Gong, K. Zhu, X.-P. Hu, D. Zhang, Y. Xu, Y.-Y. Wang, Nat. Phys. 14 (2018) 344–348.
[70] J. Falson, Y. Xu, M. Liao, Y. Zang, K. Zhu, C. Wang, Z. Zhang, H. Liu, W. Duan, K. He, H. Liu, J.H. Smet, D. Zhang, Q.-K. Xue, Science 367 (2020) 1454–1457.
[71] M.S. Bahramy, O.J. Clark, B.-J. Yang, J. Feng, L. Bawden, J.M. Riley, I. Marković, et al., Nat. Mater. 17 (2018) 21.
[72] O.J. Clark, M.J. Neat, K. Okawa, L. Bawden, I. Markovi, F. Mazzola, J. Feng, V. Sunko, J.M. Riley, W. Meevasana, Phys. Rev. Lett. 120 (2018) 156401.
[73] S. Furuseth, K. Selte, A. Kjekshus, S. Gronowitz, A. Westerdahl, Acta Chem. Scand. 19 (1965) 257–258.
[74] Y. Liu, Y. Xu, J. Sun, C. Liu, J. Wang, Nano Lett. 20 (2020) 5728–5734.
[75] F. Bergeret, A.F. Volkov, K.B. Efetov, Rev. Mod. Phys. 77 (2005) 1321.
[76] M. Eschrig, Phys. Today 64 (2011) 43.
[77] C. Beenakker, Annu. Rev. Condens. Matter Phys. 4 (2013) 113–136.
[78] Y. Zhang, H. Wang, F. Li, X. Sun, B. Dong, X. Li, Z.V. Han, T. Yang, H. Zhang, Sci. China Inf. Sci. 62 (2019) 1–27.
[79] K. Kang, S. Jiang, H. Berger, K. Watanabe, T. Taniguchi, L. Forró, J. Shan, K.F. Mak, *arXiv preprint arXiv:2101.01327* **2021**.
[80] T. Kontos, M. Aprili, J. Lesueur, F. Genêt, B. Stephanidis, R. Boursier, Phys. Rev. Lett. 89 (2002) 137007.
[81] A.I. Buzdin, L. Bulaevskii, S. Panyukov, JETP Lett. (Engl. Transl.) 35 (1982) 147.
[82] A.I. Buzdin, Rev. Mod. Phys. 77 (2005) 935.
[83] V. Ryazanov, V. Oboznov, A.Y. Rusanov, A. Veretennikov, A.A. Golubov, J. Aarts, Phys. Rev. Lett. 86 (2001) 2427.
[84] Y. Blum, A. Tsukernik, M. Karpovski, A. Palevski, Phys. Rev. Lett. 89 (2002) 187004.
[85] V. Oboznov, V. Bol'ginov, A. Feofanov, V. Ryazanov, A.I. Buzdin, Phys. Rev. Lett. 96 (2006) 197003.
[86] E. Strambini, A. Iorio, O. Durante, R. Citro, C. Sanz-Fernández, C. Guarcello, I.V. Tokatly, A. Braggio, M. Rocci, N. Ligato, Nat. Nanotechnol. 15 (2020) 656–660.
[87] E. Goldobin, H. Sickinger, M. Weides, N. Ruppelt, H. Kohlstedt, R. Kleiner, D. Koelle, Appl. Phys. Lett. 102 (2013) 242602.
[88] E. Gingrich, B.M. Niedzielski, J.A. Glick, Y. Wang, D. Miller, R. Loloee, W. Pratt Jr., N.O. Birge, Nat. Phys. 12 (2016) 564–567.
[89] R. Menditto, H. Sickinger, M. Weides, H. Kohlstedt, D. Koelle, R. Kleiner, E. Goldobin, Phys. Rev. 94 (2016): 042202.
[90] T. Park, H. Ishizuka, N. Nagaosa, Phys. Rev. B 100 (2019) 224301.
[91] I. Kulagina, J. Linder, Phys. Rev. B 90 (2014): 054504.
[92] H. Idzuchi, F. Pientka, K.-F. Huang, K. Harada, Ö. Gül, Y. Shin, L. Nguyen, N. Jo, D. Shindo, R. Cava, *arXiv preprint arXiv:2012.14969* **2020**.
[93] Z. Wang, T. Zhang, M. Ding, B. Dong, Y. Li, M. Chen, X. Li, J. Huang, H. Wang, X. Zhao, Nat. Nanotechnol. 13 (2018) 554–559.
[94] L. Ai, E. Zhang, C. Huang, X. Xie, Y. Yang, Z. Jia, Y. Zhang, S. Liu, Z. Li, P. Leng, *arXiv preprint arXiv:2101.04323* **2021**.
[95] G.C. Ménard, S. Guissart, C. Brun, S. Pons, V.S. Stolyarov, F. Debontridder, M.V. Leclerc, E. Janod, L. Cario, D. Roditchev, Nat. Phys. 11 (2015) 1013–1016.
[96] C. Kallin, J. Berlinsky, Reports on Progress in Physics Physical Society 79 (2016): 054502.
[97] X.L. Qi, S.-C. Zhang, Rev. Mod. Phys. 83 (2011) 1057–1110.
[98] Catherine Kallin, Rep. Prog. Phys. 75 (2012): 042501.
[99] F. Wilczek, Nat. Phys. 5 (2009) 614–618.
[100] A. Stern, Nature 464 (2010) 187–193.
[101] N. Read, D. Green, Phys. Rev. B 61 (2000) 10267.
[102] D.A. Ivanov, Phys. Rev. Lett. 86 (2001) 268.
[103] Y. Li, Z.A. Xu, Advanced Quantum Technologies 2 (2019) 1800112.
[104] B.T. Zhou, N.F.Q. Yuan, H.L. Jiang, K.T. Law, Phys. Rev. B 93 (2016) 180501 (R).
[105] G. Sharma, S. Tewari, Phys. Rev. B 94 (2016): 094515.
[106] J. Zhang, V. Aji, Phys. Rev. B 94 (2016): 060501.
[107] Y.T. Hsu, A. Vaezi, M.H. Fischer, E.-A. Kim, Nat. Commun. 8 (2017) 14985.
[108] W.-Y. He, B.T. Zhou, J.J. He, T. Zhang, K. Law, Preprint at, 2016. http://arxiv.org/abs/1604.02867.
[109] L. Yu, Acta Phys. Sin. 21 (1965) 75–91.
[110] S. Hiroyuki, Prog. Theor. Phys. 40 (1968) 435–451.
[111] A.I. Rusinov, J. Exp. Theor. Phys. 29 (1969) 1101.
[112] W.-Y. He, B.T. Zhou, J.J. He, N.F. Yuan, T. Zhang, K.T. Law, Commun. Phys. 1 (2018) 40.
[113] B.T. Zhou, N.F.Q. Yuan, H.-L. Jiang, K.T. Law, Phys. Rev. B 93 (2016) 180501 (R).